NIPES

Journal of Science and Technology Research

Journal homepage: www.nipesjournals.org.ng

Effect of Microstructural Morphology on the Cavity formation of 0.17%C Low Alloy Steel and 0.32%C Steel

[a]Unueroh Ufuoma Georgina, [b]Awheme Oghenerobo

[ab]University of Benin, Benin city. PMB 1154, Ugbowo Benin City

ARTICLE INFORMATION

Article history:
Received 28 February 2019
Revised 10 March 2019
Accepted 15 March 2019
Available online 25 March 2019

Keywords:
Cavity
Plastic Deformation
Carbide Particle

ABSTRACT

Carbides and non- metallic inclusions, present in steels are found to be sites for cavity formation during plastic straining. It is therefore necessary to study how the carbide particle morphology affects the formation of cavities To achieve this, the samples were spherodized and the microstructure was obtained. The samples were then prestrained into three strain level (0.3, 0.4 and 0.45), immersed in liquid nitrogen and thereafter fractured by impact. The cavities were viewed with scanning electron microscope. The results showed that the cavities produced is a direct function of the carbide volume fraction, shape and carbide particle type. The 0.17%C low alloy steel was found to have more cavities when compared to 0.32%C steel

1. Introduction

Low alloy and medium carbon steel are widely used for the construction of pipelines and other offshore structures. These pipelines are subjected to plastic deformation which results in cavities during installation. One notable engineering scenario where steel components suffer from plastic deformation due to accidental loading, cold bending, and ground movement is the pipe reeling process in offshore industries. In the reel lay process, the pipe is initially reeled onto a drum on a vessel for transportation. During installations, the pipe is unreeled, straightened and thereafter deployed into the sea. During the laying process, the pipelines are subjected to repeated plastic straining. Axial plastic deformations as large as 2% can possibly occur, making the pipe section to experience plastic strain cyclically [1, 2]. Though it is argued that during hydrostatic testing of these pipelines, the effect of plastic straining is reduced to the barest minimum. Researches have shown that plastic straining leaves lasting damages to the pipelines in the form of cavities. The micro-cavities developed as a result of the plastic deformation, acts as stress concentration sites [3-8]. Carbides and non- metallic inclusions, present in steels are found to be sites for cavity formation. These carbide and non- metallic inclusions are formed as a result of the distribution of alloying elements in steel. The distribution of these elements depends mainly on the carbon contents of steel and the presence of other carbide-forming elements. For instance, if a steel contains a great quantity of an alloying element and a relatively small amount of carbon, the carbon will be bound to carbides before the carbide forming elements are used completely. This results in excess carbide forming elements in the solid solution. If a steel though has a large amount of carbon and little of the alloying elements, the alloying elements will be present in the steel mainly as carbides [9].

Metallic carbides (MC) are usually hard and brittle. Their thermal stability does not exceed 1000-1100^{0}C. Although the MC system is very complex at elevated temperature, only $M_{23}C_6$, M_5C_6 and

M_7C_3 are said to be thermodynamically stable at ambient temperatures [10]. Most of the Metallic carbides are found to be mostly cubic in shape and gray and whitish in colour [10, 11].The colour of the precipitate however is sometimes dependent on the nature of light view. $M_{23}C_6$ for instance are white but in a lens detector, they appear dark [12].

Non-metallic inclusions are classified into several types based on their composition. They are sulphides (FeS, MnS, CaS etc.), oxides (Al_2O_3, MnO, FeO, etc), nitrides (NiN, Si_3N_4, etc), phosphides (Fe_3P, etc), carbides (Fe3C, etc) and complex inclusions. (Al_2O_3 –MnS, etc) Oxides and sulphides are however thought to be harmfull for steels in some cases. MnS are elongated in shape and usually deform into enlongated stringers. In the structural steel studied by Berzega [13], MnS stringers and oxide particles were shown to be the key damage initiation sites. They also carried out void size and porosity measurements in steel in relation to their inclusion content, elongated MnS and Al were found to be the main void nucleation sites in these materials. Their findings agree with a previous study by Chatterjee [14], who studied round and stringer shaped inclusions and observed that larger cavities were found more around the stringer shaped inclusions than the round inclusions. MnS usually forms preferentially to FeS and has a high melting point and appears as very discrete randomly distributed globules.

MnS has three types: type I (globular with a wide range of size and is often with the form of duplex oxysulphide) type II (dentritic) and type III (angular sulphide that often form single phase inclusion) [15]. According to Temmel [15], type I and III MnS inclusions may deform to a flat pancake shape, leading to the anisotrophy and high stress will be concentrated on the edge of MnS after deformation.

Most materials are heterogeneous in nature. These materials contain second phase precipitate and non-metallic inclusions. They are usually harder than the matrix. So when stress is applied to such material, The soft matrix is deformed plastically while the second phase precipitate are just beginning to deform elastically. The difference between the deformation results in the nucleation of cavities at the particle-matrix interface [16]. These cavities then grow under the influence of increasing plastic strain and high hydrostatic stress within the material [17]. For ductile materials, continuous stressing results in additional nucleation of cavities. The larger particles nucleate cavities at lower stresses and strains [18]. Smaller particles, on the other hand, starts contributing to cavity nucleation when the material is subjected to greater plastic deformation. Gao and Kim [17], who studied the effect of prestraining on cavity nucleation also agrees with these findings that cavity nucleation is usually formed at larger particles at lower strains, while smaller particles nucleate cavities as the strain is progressively increased. Blaha et al. [19], however, observed that larger single carbides are not large enough to act as critical flaws, but carbide clusters and inclusions acts as crack initiation flaws. Carbides and non-metallic inclusion in steels have been shown to be sites for cavity formation Researches have also shown that the shape, size, distribution of carbides affects the nucleation of cavities. Since carbon content and heat treatment plays a major role in the final outcome of the microstructure of a metal, there is therefore need to compare steels with varied composition, to see how they affect the formation of cavities, with a view to recommend the best steel type for use in pipeline construction.

2. Materials and Method

2.1. Materials

A 20mm diameter rod was used for this investigation. The chemical composition for 0.17%C low alloy and 0.32%C steel are shown in Table 1.

Table 1. Chemical composition of the investigated steels.

Element	C	Si	Mn	S	P	Cr	Ni	Cu	Nb	Al	B	W	Mo	V	Ti	Co	Tn	Sn	As	Pb	Fe
Steel 1 (Wt-%)	0.17	0.3	1.2	0	0	0.26	0.12	0.3	0.02	0.01	0.005	0.05	0.01	0.01	0.01	0.02	0.01	0.01	0.01	0.02	97.6
Steel 2 (Wt-%)	0.32	0.3	0.9	0.1	0.1	0.11	0.13	0.3	1E-04	0.001	0.002	0.0001	0.0001	1E-04	1E-04						97.6

2.2. Spherodizing

The specimens were first heat treated to an austenizing temperature. The medium carbon steel was heated to 850^0C and held for 25 minutes in a muffle furnace and then quenched in water. The low alloy steel was equally heat treated to 820^0C for 25 minutes and quenched in water. After quenching, both steels were subsequently placed in the muffle furnace at 650^0C respectively. The austentizing temperature of the low alloy steel was determined by using the carbon equivalent number formular in Equation 1 and inputing the parameters in Steel 1 on Table 1

$$CE = C + \frac{Cr+Mo+V}{5}\frac{(Cr+Mo+V)}{5} + \frac{Mn+Si}{6}\frac{(Mn+Si)}{6} + \frac{Ni+Cu}{15} \quad (1)$$

Where, CE is the Carbon Equivalent Weight Percentage.

Imputing the values from Table 3.2 in equation 3.1, we have

$$CE = 0.17 + \frac{(0.2559+0.01+0.01)}{5} + \frac{(1.2089+0.3016)}{6} + \frac{(0.1218+0.2560)}{15}$$

$$CE = 0.17 + 0.05518 + 0.25775 + 0.02519$$

$$CE = 0.50212\%C$$

2.3. Microstructural characterization

The specimens were grinded with various grits of emery paper and then polished on a rotating wheel. 2% Nital was used to etch the specimens. The surfaces were then examined in an optical microscope. The metallographic examination was conducted at Petroleum Training Institute Effurun. The results are shown in Figure 3a and 3b

2.3.1. Volume Fraction Evaluation: Stereology

In order to determine the effect of carbide formation in the microstructure on the cavities induced on the fracture surfaces of the specimens at various prestrain levels and on corrosion, Stereology was adopted. Stereology is a universally accepted method that is used to evaluate volume fraction of phases in a microstructure as a result of its simplicity and reliability [20]. Various magnifications of X400, X750 and X1000 were used to examine the microstructure. Five 7x7 point grid was then placed on the X1000 specimen different part of each micrograph. An example of the grid used for all the measurement is shown in Figure 4a.

2.3.2. Carbide Particle Size Evaluation: Stereology

The carbide particle sizes were evaluated to determine how the sizes relate to the formation of cavities. This was done by using the intercept method according to the American standard method for measuring grain size. (ASTM 112-12) Seven lines of equal length were drawn on the surface of the microstructure. The points where the test line intercept with the carbide particle boundary is counted as 1 point. A tangential intersection with a carbide particle boundary is counted as one intersection, while an intersection coinciding with the junction of three grains is scored as one and a half. The points of intersection for the investigated steels are shown in Table 3 and 4. An example of the lines drawn is shown in Figure 4a. Equations 2 to 7 were used to calculate the diameter of the carbide sizes.

$$Mean\ Intercept\ Length\ (\bar{l}) = \frac{Total\ Length}{No\ of\ Intersection\ x\ Magnification} \quad (2)$$

$$ASTM\ Grain\ Size\ Parameter\ G = 6.6439 Log_{10}(\bar{l}) - 3.288 \quad (3)$$

$\bar{l}$ is mean intercept length in mm

$$n = 2^{G-1} \quad (4)$$

n is the number of grains visible in the microstructure per in^2

Assuming the grains are spherical

$$\bar{a} = \frac{2}{3}\pi r^2 \quad (5)$$

$$\bar{a} = \frac{1}{N_A} \quad (6)$$

$\bar{a}$ is the average area of grain

N_A is the Number of grains per unit area

$$d = 2\left(\frac{3}{2}\frac{\bar{a}}{\pi}\right)^{1_2} \quad (7)$$

2.3.3. Statistical Analysis

Since no determination of the average grain size can be an exact measurement, there is need to evaluate the precision within which the determined size may with normal confidence, be said to represent the actual average carbide particle size of the specimen examined.

Standard Deviation (SD). This is used to determine how measurements for a group are spread out from the average mean. A low standard deviation shows that most of the number are very close to the average, while a high standard deviation means that the numbers are spread out.

$$SD = \left(\frac{\sum(x-\bar{x})^2}{n-1}\right)^{\frac{1}{2}} \quad (8)$$

Standard Error (SE). This is the deviation of the sample mean from the actual mean

$$SE = \frac{SD}{\sqrt{n}} \quad (9)$$

95% Confidence Interval (95%CI). 95% confidence interval represents 95% of the mean values that will be obtained. If the test is conducted 100 times, the average values would be between plus and minus the average mean in 95 of the measurement

$$95\%CI = \underline{X} \pm 2SE \quad (10)$$

2.4. Notched Tensile Specimens.

The specimens were machined into tensile test specimens according to the American society for Testing and Materials Specifications. (ASTM 2014) The tensile specimens geometry and dimensions are shown in Figure 5 and was prepared according to ASTM A370-14 Standard

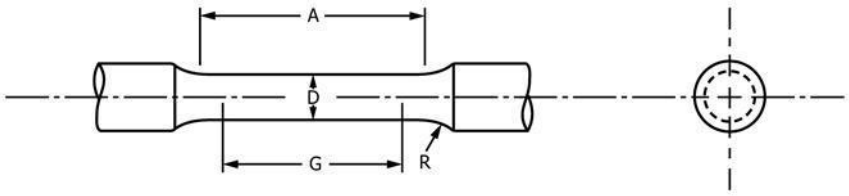

Figure 1: ASTM A370 – 14 Tensile Sample

Where A = Length of reduced section. (100mm)
D = Diameter of guage length. (12.5mm)
G = Guage length. (50mm)
R = Radius of fillet. (2mm)

To localize damage, circumferential v-notched were machined on the round bar tensile specimens. In notched tensile specimens, the load is concentrated in the core of the notch. When load is applied, the unstressed mass of the material tends to resist the deformation of the central core. This produces radial and tranverse stresses and a triaxial state of stress in the notch region, leading to stable cavity formation at the particle-matrix interface (21). Notched bars are able to reach high level of deformation so that the hardening behaviour is determined over a wide range for plastic strain. This presents an advantage over the sole use of smooth tensile bars which need to be analyzed beyond necking to reach high deformation levels. [22]

A circumferential V- notch of angle 60 was machined to a depth of 1.5mm at the centre of some of the specimens. The notch radius was as small as possible (0.075mm) The machining of the V-notch on the specimens were achieved by using a programmable lathe machine.

Figure 2: A picture of the notched specimen used for this research

2.5. Prestraining

In order to observe the effect of prior plastic deformation on the specimens, the notched specimens were prestrained to three different prestrain levels. To achieve this prestrain values, some notched specimens were fractured to failure. Strain guages were glued on the surface of tested specimens and connected to a strain meter to check the actual strain levels before fracture. They were prestrained to 0.3, 0.4 and 0.45.

2.6. Fracturing with Nitrogen Gas

In order to fully characterized ductile damage on the fracture surfaces of the specimens prestrained at room temperature, some specimens prestrained at the various strain levels, were immersed in liquid nitrogen at -196^{0}C and thereafter fractured in a bench vice.

2.7. Cavity Distribution

To measure the cavity distribution, the number of cavities seen on the fracture surfaces was counted. The cavity density was then evaluated and expressed as Average Nearest Neighbour Distance (A.N.N.D), which is defined as

$$\text{A.N.N.D} = \left[\frac{Surface\ area}{No\ of\ Cavities}\right]^{\frac{1}{2}}\mu m \qquad (11)$$

The surface area was calculated by using the diameter of the field of view (FOV) found in the SEM images. The number of cavities was counted manually and the average value was taken after 4 counts. The cavity sizes produced during the plastic strain history were measured manually using digital venial caliper. The mean cavity sizes at different prestrain levels and the number of cavities for both steels are shown in Table 5

3. Results and Discussion

3.1. Microstructural Evaluation

The microstructure of 0.17%C Low alloy and 0.32%C steel is shown in Figure 3. An example of the Grid used in the Carbide Volume Fracture Evaluation and an example of the lines used in the line intercept method is also shown in Figure 4. Table 2 shows the carbide volume fracture values. Table 3 and 4 shows the number of intersections for 0.32%C and 0.17%C low alloy steel specimens respectively

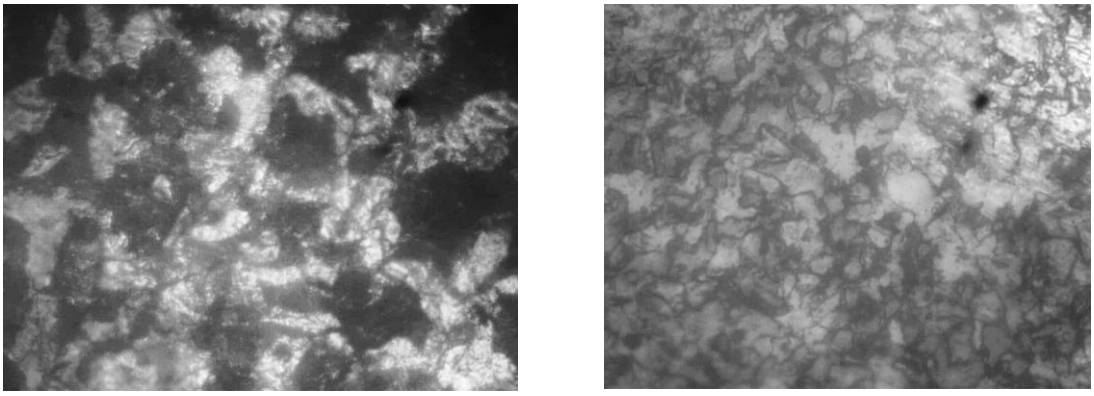

a b

Figure 3. Microstructure of the investigated steels **(a).** 0.32%C **(b).** 0.17%C

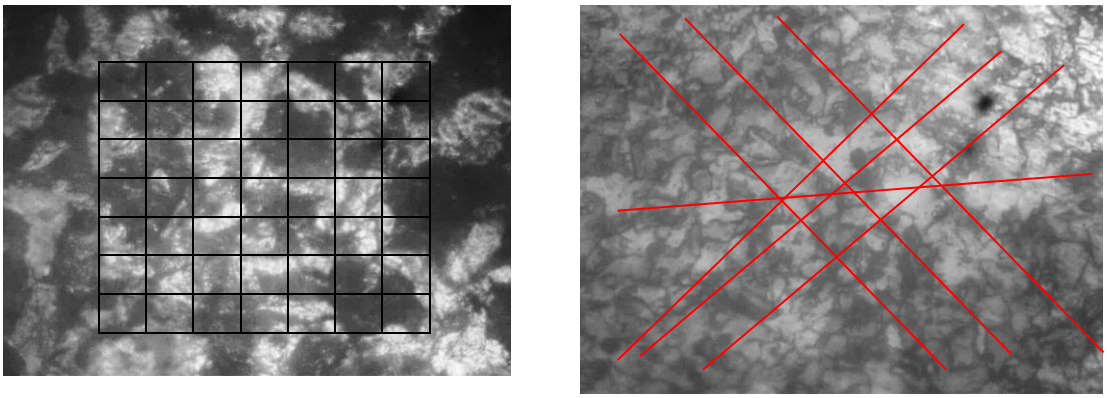

a b

Figure 4: (a). An example of grid used for Carbide Volume Fracture. **(b).** An example of lines used for the line intercept method

Table 2: Analysis of Carbide Volume Fraction Measurement

Steel Type	Sample Number	Carbide Volume Fraction [CVF] (%)				
		CVF Per Sample (%)	Mean	Standard Deviation	Total Mean	Total Standard Deviation
0.17%C	1	59,49,51,57,45	52.2	5.15	53.00	5.89
	2	55,51,59,45,49	51.8	4.82		
	3	63,41,53,59,59	55	7.69		
0.32%C	1	47,43,55,49,37	46.2	6.01	46.01	5.57
	2	49,41,41,43,47	44.2	3.25		
	3	37,51,55,41,55	47.8	7.44		

Table 3: No of intersections for 0.32%C Steel (Line Intercept Method)

Line No	No of intersection (X)	Mean ($\bar{X}$)	($X - \bar{X}$)	$(X - \bar{X})^2$
1	8	13.29	-5,29	27.98
2	11	13.29	-2.29	05.24
3	12	13.29	-1.29	01.66
4	19	13.29	5.71	32.60
5	11	13.29	-2.29	05.24
6	16	13.29	2.71	07.34
7	16	13.29	2.71	07.34
			$\sum(X - X)^2$	87.4

From Equation 8, Standard Deviation SD = $\left(\frac{87.4}{6}\right)^{1_2} = 3.817$

From Equation 9, Standard Error SE $= \frac{3.8167}{\sqrt{7}} = 1.44$

From Equation 10, 95%Confidence Interval 95%CI$= 13.29 \pm 2(1.44)$

= 10.41 to 16.17

Table 4: No of intersections for 0.17%C Low Alloy Steel (Line Intercept Method)

Line No	No of intersection (X)	Mean ($\bar{X}$)	($X - \bar{X}$)	$(X - \bar{X})^2$
1	25	23.43	1.57	02.46
2	23	23.43	-0.43	00.18
3	23	23.43	-0.43	00.18
4	27	23.43	3.57	12.74
5	23	23.43	-0.43	00.18
6	24	23.43	0.57	00.32
7	19	23.43	-4.43	19.62
			$\sum(X - X)^2$	35.68

From Equation 8, Standard Deviation SD = $\left(\frac{35.68}{6}\right)^{1_2} = 2.439$

From Equation 9, Standard Error SE $= \frac{2.439}{\sqrt{7}} = 0.922$

From Equation 10, 95%Confidence Interval 95%CI$= 23.43 \pm 2(0.922)$

= 21.59 to 25.27

3.1.1 Determination of Medium Carbon Steel Carbide Particle Size

From Equation 2, Mean Intercept Length $\underline{I} = \frac{7\ X\ 145}{93\ X\ 100X} = 0.109mm$

Each test line drawn on the microstructure is 145mm

From Equation 3, grain size parameter G $= -6.644(log\ log\ 0.109) - 3.288$

$= 3.11$

From Equation 4, $n = 2^{3.11-1}$

$= 4.32Inch^2$

$= 2787.0912mm^2$

Inch^2 = 645.16mm^2

From Equation 6 $\underline{a} = \frac{1}{2787.0912} = 0.00036mm^2$

From Equation 7, $d = 2\left(\frac{3\ x\ 0.00036}{6.283}\right)^{1_2}$

= 26μm

3.1.2 Determination of Low Alloy Steel Carbide Particle Size

From Equation 2, Mean Intercept Length $\underline{\boldsymbol{I}} = \frac{7\ X\ 145}{164\ X\ 100X} = \mathbf{0.062}\boldsymbol{mm}$

Each test line drawn on the microstructure is 145mm

From Equation 3, grain size parameter $G = -6.644(log\ log\ 0.062) - 3.288$

$= 4.74$

From Equation 4, $= 2^{4.74-1}$

$= 13.36\boldsymbol{Inch^2}$

$= 8619.3376\boldsymbol{mm^2}$

Inch^2 = 645.16mm^2

From Equation 6, $\underline{\boldsymbol{a}} = \frac{1}{8619.3376} = 0.00012\boldsymbol{mm^2}$

From Equation 7, $\boldsymbol{d} = 2\left(\frac{3\ x\ 0.00012}{6.283}\right)^{1_2}$

= 15μm

3.2. Cavity Evaluation Result

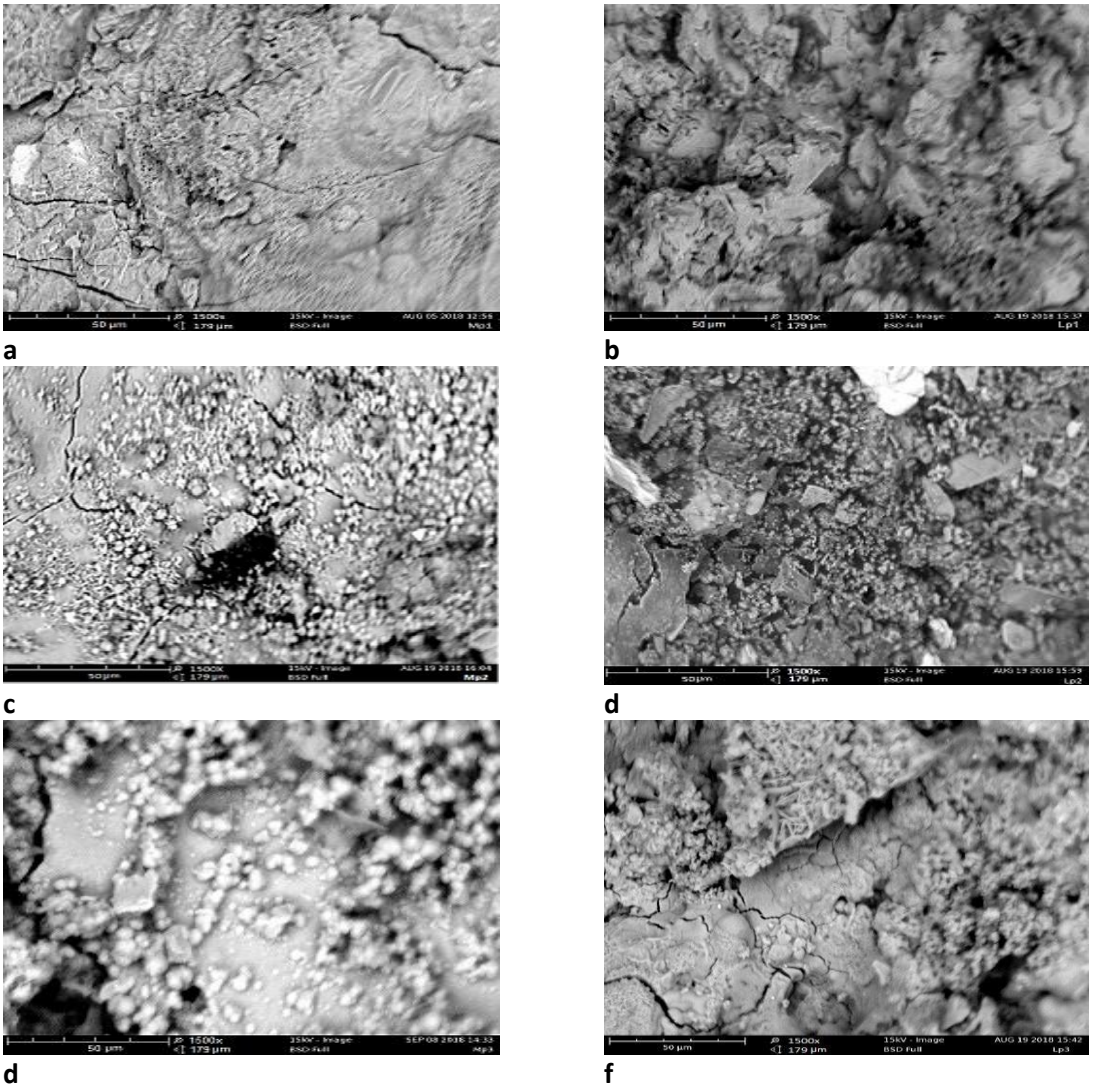

Figure 5: Cavity Formation at Three Different Prestrain Levels for the Investigated Steel **(a).** 0.32%C Steel- Prestrain 0.3. **(b).** 0.17%C Low alloy Steel-Prestrain 0.3 **(c).** 0.32%C Steel-Prestrain 0.4. **(d).** 0.17%C Low alloy Steel- Prestrain 0.4 **(e).** 0.32%C Steel- Prestrain 0.45. **(f).** 0.17%C Low alloy Steel- Prestrain 0.45

Table 5: Cavity size, Number of Cavity and Average Nearest Neighbor Distance (ANND)

Samples	Mean Cavity Size (µm)	Range of Cavity Sizes	ANND								
			Ist Count		2nd Count		3rd Count		4th Count		
			No of Cavities	ANND (µm)	No of Cavities	ANND (µm)	No of Cavities	ANND (µm)	No of Cavities	ANND (µm)	Mean ANND (µm)
Lp_1	0.76	0.13-2.07	38	25.75	38	25.75	40	25.08	40	25.08	25.42
Lp_2	1.03	0.13-3.47	42	24.47	42	24.47	44	23.91	44	23.11	24.19
Lp_3	1.37	0.13-4	46	23.38	47	22.65	45	23.64	47	22.65	23.08
Mp_1	0.4	0.04-1.33	26	31.1	29	29.45	26	31.1	27	30.52	30.54
Mp_2	0.75	0.04-2.87	40	25.08	38	25.75	38	25.75	38	25.75	25.58
Mp_3	1.2	0.06-3.33	42	24.47	44	23.38	42	24.47	44	23.38	23.93

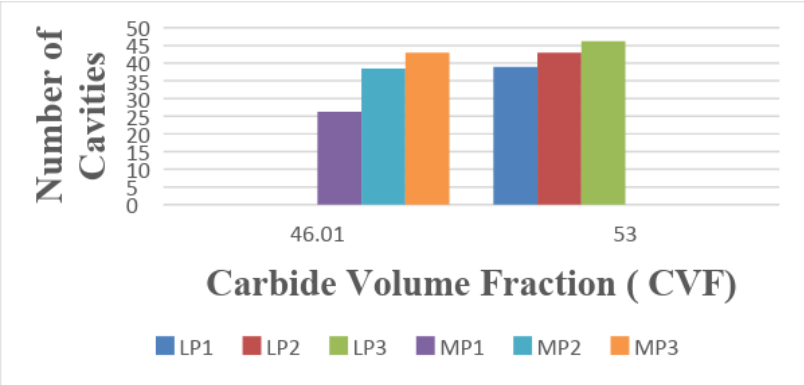

Figure 6: A Graph showing the Number of Cavities against the Carbide Volume Fracture for the Investigated Steel

3.3. Cavity Examination Result

The fracture surfaces of the prestrained samples were immersed in liquid nitrogen at -196^{0}C and thereafter, fractured by impact, to fully characterize the cavities obtained. They are shown in Figure 5a to 5f (Figure 5a,5c and 5e are 0.32%C steel samples, while Figure 5b, 5d and 5f are 0.17%C steel samples) Figure 5a shows cavities that are concentrated in a particular area. The cavities are smaller in size and more circular in shape when compared with Figure 5b, both prestrained at 0.3. Figure 5c shows more stringer shaped cavities that appear to be nucleated and fully distributed within the grain and the grain boundaries. Figure 5d shows more round shaped cavities that are growing in size with smaller cavities nucleating. Globular shaped precipitate is also observed within the surfaces. Figure 5e on the other hand shows more stringer shaped cavities growing, resulting in increase in sizes with smaller cavities nucleating. Cubic shaped precipitate is also observed within the surface. Figure 5e prestrained at 0.45 shows more circularly shaped cavities with sizes bigger than cavities in Figure 5c, strained at 0.4. Some of the cavities are already linking causing cracks propagating along the grain boundaries, while Figure 5f shows more stringer shaped cavities with sizes that appear bigger than that of Figure 5d. It also shows some cracks propagating along the grain boundary as a result of cavities linking.

3.4. Effect of Microstructural Morphology on the Formation of Cavities

Figure 3a and 3b shows the microstructure of 0.32%C and 0.17%C low alloy steel. Figure 3a shows majorly almost spheroidal carbides that are evenly distributed in the ferrite matrix (Light Phase) Figure 3b on the other hand, shows an irregularly shaped/stringer shaped spheroidal carbides and more inclusions that are more concentrated at the ferrite matrix and also at the grain boundaries. The carbides also appear to be more clustered as against Figure 3a, where the carbides are more apart from each other. Figure 3b also appears to have greyer phase than Figure 3a. This grey phase present in the microstructure is possibly as a result of some specific type of carbides present in these steels [10, 12].

The average carbide particle size diameter for the low alloy steel is 15μm, while the medium carbon steel is 26μm. The sizes did not seem to have a direct relationship with the sizes of the cavities obtained, it is possible however, that the smaller sizes of the low alloy steel samples could have resulted in more cavities being nucleated. Although it was observed that larger particles nucleate at lower stresses and strains, while smaller particles on the other hand starts contributing to cavity nucleation when the material is subjected to greater deformation [17, 18]. The higher yield stress of the low alloy steel could have resulted in cavities being nucleated at smaller carbide particle sites at a lower plastic strain. The 95% confidence interval shows that in 95 of the measurement of the actual average mean interception taken, the values will be between 10.41 to 16.17, for medium carbon steel sample and 21.59 to 25.27, for low alloy steel sample. This shows a high level of accuracy for the values gotten.

The carbide particle type, shape and distribution within the ferrite matrix, however played a major row in the cavities produced. The 0.17%C low alloy steel contain more Mn, some of which formed MnS. MnS have been shown to be enlongated in shape and deform into enlongated stringers [13]. This explains why there are more enlongated stringer shaped cavities in the low alloy steel than in the medium carbon steel. The stringer shaped or irregularly shaped carbides in Figure 3b played a major role in more cavities being nucleated in Figure 5b, 5d and 5f for the low alloy steel. This is so because Mns stringer and oxide particles have been shown to be the key cavity initiation sites. This finding also agrees with Chatterjee [14], who studied round and stringer shaped inclusions and discovered that larger cavities were found more around stringer shaped inclusions than the round inclusions. Another factor that could have also played a major role in more cavities being nucleated in the low alloy steel is the manner in which the carbides and inclusions are distributed within the ferrite matrix. The carbides and inclusions in the 0.17%C are more clustered together. The impact of the strain on these carbides could have possibly resulted in quick transfer of cavities from cavity nucleation site to another, since they are closely linked together. These findings agrees with Blaha et al. [19], who observed that larger single carbides are not large enough to act as critical flaws, but carbide clusters and inclusions acts as crack initiation flaws.

Globular shaped, whitish precipitate was observed within the surfaces of some of the cavity (Figure 5c, 5e and 5f). Some of the cavity surfaces also contain cubic shaped precipitate (Figure 5a and 5d). This cubic precipitate is mostly observed in the low alloy steel cavity surfaces. Some of them appear grey and whitish in colour. This observation is in line with the findings of Karen et al. [10], Tchuindjang and Lecomte-beckers [11]. They observed that Metallic carbides are mostly cubic and globular in shape and grey and whitish in colour.

3.5. Effect of Carbide Volume fraction (CVF) on Cavity distribution

Table 2 shows the mean carbide particle volume fraction for low alloy steel and medium carbon steel. Figure 6 on the other hand shows a plot of carbide volume fraction against number of cavities. Table 2 shows that the carbide volume fraction for low alloy steel is greater than that of medium carbon steel. The higher CVF of low alloy steel accounts for more cavities to be formed in the steel as shown in Figure 6 which shows a decline in the mean number of cavities for medium carbon steel as against low alloy steel at all prestrain levels. One major reason for this could be as a result of the fact that cavities are nucleated at the second phase precipitate by

decohension at the particle matrix interface or by particle cracking (16). Low alloy steel will have more sites for cavity nucleation as a result of the higher percentage of carbides and inclusions present in it. The findings also agrees with Bhadeshia and Honeycombe [9], who observed that for steels with more alloying elements than carbon, carbon will be bound to carbides before the alloying elements are exhausted, resulting in excess carbide forming elements in the solid solution.

The low standard deviation values of the CVF for both steels show that most of the data taken are close to the average. The lower value for the medium carbon steel sample (5.57) shows that the carbide particle are closely parked or evenly distributed. The low alloy steel on the other hand, had a higher standard deviation value (5.89). This shows that the carbide particles are spread out within the ferrite matrix. This is in line with the visual observation of the microstructure.

4. Conclusion

The research show that the carbide sizes had effect on the degree of cavities formed. It was however observed that the carbide distribution, carbide volume fraction, carbide particle type and shape played a significant role in the nature of cavities formed. The low alloy steel was found to have more cavities as a result of its carbide particle type, shape and carbide volume fraction.

5. Acknowledgement

The Authors wish to acknowledge Professor Basil O. Onyekpe for his Academic input.

6. Conflict of Interest

There is no conflict of interest associated with this work.

References

[1] Zhang, Z. L and Skallerud B. (2010): Coalescence with and without prestrain History, International, *Journal of Damage Mechanics*, 19, pp153-174

[2] Vitali, L., Torselletti, E., Marchesani, F. and Bruschi R. (2005): Strain Based design for land high grade pipelines in harsh environment, *Proceedings Super-High Strength Steels*, pp2-4

[3] Chae, D., Bandstra, J.P and Koss, D. A. (2000): The Effect of Prestrain and Strain-Path Changes on Ductile Fracture: Experimental and Computational Modelling, *Materials Science and Engineering A.* 285, pp165-171

[4] Silvaprasad, S., Tarafder, S., Ranganath, V.R and Ray k. k. (2000): Effect of Prestrain on the Fracture Toughness of HSLA Steels, *Materials Science and Engineering A,* 284, pp195- 201

[5] Fakuda, N., Hagiwara, N and Masuda, T. (2005): Effect of Prestrain on Tensile and Fracture Properties of Pipelines, *Journal of Offshore Mechanics and Artic Engineering,* 127, pp263- 268

[6] Qui, H., Enoki, M., Hiraoka, K and Kishi T. (2005): Effect of Prestrain on Fracture Toughness of Ductile Structural Steels Under Static and Dynamic Loading, *Engineering Fracture Mechanics*, 72, pp1624-1633

[7] Cosham, A. (2001): A Model of Prestrain Effects on Fracture Toughness, *Journal of Offshore Mechanics and Artic Engineering,* 123, pp182-190

[8] Enami K. (2005): The Effect of Compressive and Tensile Prestrain on Ductile Fraction Initiation in Steels, *Engineering Fracture Mechanics*, 72(7), pp1089-1105

[9] Bhadeshia, H. and Honeycombe, R. (2017): Steels: Microstructure and Properties. Butterworth-Heinemann.

[10] Karen, P., Fjellvig, A., Kjekshus A and Andreson A.F (1991): On the Phase Relations and Structural and Magnetic Properties of the Stable Manganese Carbides. $Mn_{23}C_6$, Mn_5C_2 and Mn_7C_3, *Acta Chemica Scandinavica,* 45(199), pp549-557

[11] Tchuindjang, J.T. and Lecomte-Beckers, J. (2003): Inclusions and carbides characterisation in high-speed steels. *Proceedings de la journée de la société belge de microscopie (SBM-BVM), RUCA, UA.*

[12] Yadav, S.D., Sonderegger, B., Sartory, B., Sommitsch, C. and Poletti, C. (2015): Characterisation and Quantification of Cavities in 9Cr Martensitic Steel for Power Plants. *Materials Science and Technology*, *31*(5), pp.554-564.

[13] Benzerga, A.A., Besson, J. & Pineau, A. (2004a): Anisotropic Ductile Fracture. PartI: Experiments, *Acta Materialia*, 52, pp 4623-4638.

[14] Chatterjee, A., 1986. Hydrogen Degradation of Plain Carbon and Low Alloy Steels (Doctoral Dissertation, The Ohio State University).

[15] Temmel, C., Karlsson, B and Ingestion N.C. (2006): Fatigue Anistropy in Cross –Rolled Hardened Medium Carbon Steel Resulting From MnS Inclusions, *Metallurgical and Materials Transactions A*, Vol 37A, pp2995-3007.

[16] Joly, P., Cozar, R., & Pineau, A. (1990): Effect of Crystallographic Orientation of Austenite on the Formation of Cleavage Cracks in Ferrite in an Aged Duplex Stainless Steel, *Scripta Metallurgica Materials*, 24, pp2235–2240.

[17] Gao, X. and Kim, J. (2006): Modeling of Ductile Fracture: Significance of Void Coalescence, *International Journal of Solids and Structures*, 43 (20), pp6277-6293

[18] Goods, S.H. and Brown, L.M. (1979): The nucleation of cavities by plastic deformation, *Acta metallurgica*, *27*(1), pp.1-15.

[19] Blaha, J., Krempaszky, C., Werner, E.A. and Liebfahrt, W. (2002): September. Carbide Distribution Effects in Cold Work Tool Steels. In *6th International Tooling Conference*, pp. 289-298 Karlstadt University, Schweden.

[20] Russ J.C and Dehoff R.T. (1999): Practical Stereology. 2nd Ed. *Plenum Press*, New York

[21] Onyekpe, B.O. and Wright, J.O (1983): The Influence of Hydrogen on Plain Carbon and Low Alloy Steel Containing Strain Induced Cavities, International Journal of Fracture, 22, pp231-239

[22] Mirone, G. (2004): A new model for the elastoplastic characterization and the stress–strain determination on the necking section of a tensile specimen. *International Journal of Solids and Structures*, *41*(13), pp.3545-3564.